CANCER GENOMICS & PROTEOMICS *19*: 711-726 (2022)
doi:10.21873/cgp.20354

Novel *TPR::ROS1* Fusion Gene Activates MAPK, PI3K and JAK/STAT Signaling in an Infant-type Pediatric Glioma

LILY DELAND[1,2], SIMON KEANE[3], THOMAS OLSSON BONTELL[4,5], HENRIK FAGMAN[2,4], HELENE SJÖGREN[1], ANDERS E. LIND[6], HELENA CARÉN[7], MAGNUS TISELL[8], JONAS A. NILSSON[9], KATARINA EJESKÄR[3], MAGNUS SABEL[10,11] and FRIDA ABEL[1,2]

[1]*Department of Clinical Genetics and Genomics, Sahlgrenska University Hospital, Gothenburg, Sweden;*
[2]*Department of Laboratory Medicine, Institute of Biomedicine, Sahlgrenska Academy, University of Gothenburg, Gothenburg, Sweden;*
[3]*Translational Medicine, School of Health Sciences, University of Skövde, Skövde, Sweden;*
[4]*Department of Clinical Pathology, Sahlgrenska University Hospital, Gothenburg, Sweden;*
[5]*Institute of Neuroscience and Physiology, Sahlgrenska Academy, University of Gothenburg, Gothenburg, Sweden;*
[6]*Clinical Genomics Gothenburg, SciLife Labs, Sahlgrenska Academy, University of Gothenburg, Gothenburg, Sweden;*
[7]*Sahlgrenska Center for Cancer Research, Institute of Biomedicine, Sahlgrenska Academy, University of Gothenburg, Gothenburg, Sweden;*
[8]*Department of Clinical Neuroscience and Rehabilitation, Sahlgrenska University Hospital, Gothenburg, Sweden;*
[9]*Sahlgrenska Center for Cancer Research, Department of Surgery, Institute of Clinical Sciences, Sahlgrenska Academy, University of Gothenburg, Gothenburg, Sweden;*
[10]*Childhood Cancer Centre, Queen Silvia Children's Hospital, Sahlgrenska University Hospital, Gothenburg, Sweden;*
[11]*Institute of Clinical Sciences, Sahlgrenska Academy, University of Gothenburg, Gothenburg, Sweden*

Abstract. *Background/Aim: Although fusion genes involving the proto-oncogene receptor tyrosine kinase ROS1 are rare in pediatric glioma, targeted therapies with small inhibitors are increasingly being approved for histology-agnostic fusion-positive solid tumors. Patient and Methods: Here, we present a 16-month-old boy, with a brain tumor in the third ventricle. The patient underwent complete resection but relapsed two years after diagnosis and underwent a second operation. The tumor was initially classified as a low-grade glioma (WHO grade 2); however, methylation profiling suggested the newly WHO-recognized type: infant-type hemispheric glioma. To further refine the molecular background, and search for druggable targets, whole genome (WGS) and whole transcriptome (RNA-Seq) sequencing was performed. Results: Concomitant WGS and RNA-Seq analysis revealed several segmental gains and losses resulting in complex structural rearrangements and fusion genes. Among the top-candidates was a novel TPR::ROS1 fusion, for which only the 3' end of ROS1 was expressed in tumor tissue, indicating that wild type ROS1 is not normally expressed in the tissue of origin. Functional analysis by Western blot on protein lysates from transiently transfected HEK293 cells showed the TPR::ROS1 fusion gene to activate the MAPK-, PI3K- and JAK/STAT- pathways through increased phosphorylation of ERK, AKT, STAT and S6. The downstream pathway activation was also confirmed by immunohistochemistry on tumor tissue slides from the patient. Conclusion: We have mapped the activated oncogenic pathways of a novel ROS1-fusion gene and broadened the knowledge of the newly recognized infant-type glioma subtype. The finding facilitates suitable targeted therapies for the patient in case of relapse.*

Correspondence to: Frida Abel, Assoc. Prof., Ph.D., Clinical Laboratory Geneticist, Department of Clinical Genetics and Genomics, Laboratory Medicine, Sahlgrenska University Hospital, Medicinaregatan 3B, 413 90 Gothenburg, Sweden. Tel: +46 (0)313434800, e-mail: frida.abel@gu.se

Key Words: Pediatric glioma, precision medicine, tyrosine kinases, TKI, chromosomal rearrangement, childhood cancer.

The most common solid malignancies of childhood are tumors of the central nervous system (CNS). Glioma comprises the largest group of CNS tumors among these patients (40-50%),

which are divided into pediatric high-grade (pHGG) and low-grade gliomas (pLGG) (1, 2).

Pediatric low-grade glioma, classified as grade 1 and 2 by the World Health Organization, accounts for approximately one third of brain tumors in children (1, 3). Although prognosis for these patients is generally good (>10-year overall survival between 70-96%) (2), survivors of pediatric glioma often suffer psycho-social, cognitive, neurological and endocrine complications from the tumor and/or therapy (4). New targeted therapies offer the ability for tumor control with greatly reduced toxicities, especially for inoperable or progressive pLGG (5). Pediatric brain tumors often harbor chromosomal rearrangements leading to fusion genes. The *KIAA1549::BRAF* fusion is the most prevalent, found in over a third of all pLGG and in 70-80% of pilocytic astrocytomas (grade 1) (5, 6). Other alterations in pLGG include other *BRAF*-fusions (7), *BRAF*V600E mutations (8), *FGFR1/2* fusions, mutations or duplications (9, 10), *RAF1* fusions (11), or *MYB/MYBL1* variants (12-14). The oncogenetic alterations in pLGG are mutually exclusive leading to a common theme of Mitogen-Activated Protein Kinase (MAPK) pathway activation (15). A subset of pLGG harbor fusion genes involving other receptor tyrosine kinases (RTK) *e.g., ALK*, *MET, NTRK1/2/3* and *ROS1*, and these are more frequently seen in infantile hemispheric high-grade glioma (16-18). The RTK-fusions also activate additional oncogenic pathways, such as phosphoinositide 3-kinase (PI3K) and Janus kinases (JAK)/STAT. Recent reports have found that RTK-driven (*ALK*/*MET*/*NTRK*/*ROS1*) infantile hemispheric glioma have poorer clinical outcome than those that are MAPK-driven (*BRAF*/*FGFR*-driven) (16). Targeted therapies for *ALK, NTRK* or *ROS1* fusion-driven tumors have been developed in clinical studies for different forms of solid tumors, with several approved RTK inhibitors: *e.g.,* crizotinib, entrectinib, larotrectinib and lorlatinib (19). In this study, we have characterized the molecular events driving oncogenesis in a recurrent brain tumor of a young boy with a novel *TPR::ROS1* fusion gene. The aim was to map the downstream pathways of this novel fusion and to identify potential targets for precision medicine.

Patients and Methods

Ethics approval and consent to participate. The patient's parents provided written informed consent for participation and the publication of this study, and the Medical Ethics Committee of the Sahlgrenska University Hospital, Gothenburg, Sweden, approved the study (2013-05-22; Dnr 239-13).

Patient material. The patient material used in this study was fresh frozen tumor tissue from the first operation in 2018, and formalin fixed paraffin embedded (FFPE) tumor tissue from the first and the second operation in 2020.

Clinical routine analyses. Hematoxylin and eosin staining of FFPE tumor sections were performed for routine pathological examination and assessment of tumor cell content. Immunohistochemistry (IHC) staining with antibodies against GFAP, Ki-67/MIB-1, MAP2, S100, NeuN, synaptophysin, chromogranin, TTF1, EMA, CD34, vimentin and Olig2. Ki-67/MIB-1 proliferation index was calculated manually from four different representative areas from each operation (1,64 mm^2 per operation in total, corresponding to 11,075 cells from the primary surgery and 7,352 cells from the second surgery). *BRAF*-, and *IDH1/IDH2* mutation status were assessed by Ion AmpliSeq™ Cancer Hotspot Panel v2 (Thermo Fisher Scientific, Waltham, MA, USA). H3K27M mutation status was assessed by IHC with antibody against H3 K27M. *BRAF* fusion status was evaluated by RT-PCR of the four most common *KIAA1549::BRAF* fusion junctions.

DNA and RNA extraction. Prior to DNA and RNA extraction, fresh frozen tissue was homogenized with steel bead on TissueLyser LT (Qiagen) at 30 Hz for 40 s. DNA was then extracted from approximately 10 mg fresh frozen tumor tissue using Qiagen DNeasy Blood & Tissue Kit (Qiagen, Hilden, Germany) according to manufacturer's instruction, yielding 16,7 μg of high-quality genomic DNA (A260/A280 ratio of 1.96; Lunatic spectrophotometer, Unchained Labs, Pleasanton, CA, USA). RNA was extracted from approximately 8 mg fresh frozen tumor tissue with SV Total RNA Isolation System (Promega, Madison, WI, USA) according to manufacturer's instruction, yielding 256 ng of high-quality total RNA [A260/A280 ratio of 2.24; RNA integrity number (RIN) of 8.9; DeNovix DS-11 Spectrophotometer, DeNovix, Wilmington, DE, USA and Agilent 2200 TapeStation System, ScreenTape Assay, Agilent Technologies Inc., Santa Clara, CA, USA, respectively]. RNA from FFPE was extracted from 10x5 μm tumor tissue sections using RNeasy FFPE kit (Qiagen) according to manufacturer's instructions, yielding 5.5 μg (A260/A280 ratio of 1.9; DeNovix photospectrometer).

Whole genome sequencing. Paired whole genome sequencing (WGS) was performed starting with 1 μg DNA from fresh frozen tumor tissue (T; somatic) from the first operation, and 1 μg DNA from the patient's normal blood lymphocytes (N; germline) with TruSeq DNA PCR-Free library preparation according to manufacturer's instruction. Samples were sequenced with 2*151 bp pair-end reads using the S4 std reagent kit (300 cycles) on NovaSeq 6000 (Illumina®, San Diego, CA, USA), resulting in a mean vertical coverage of 131× for tumor DNA and a mean vertical coverage of 34× for DNA from blood lymphocytes. Reads were mapped to human reference genome hs37d5/hg19, and single nucleotide variants (SNVs) and small insertion/deletions (indels) variant calling was performed using the Sentieon suite of bioinformatical tool TNscope [Sentieon Inc, Mountain View, CA, USA (20)] supplying the normal sample to filter out germline variants. Machine learning models developed by Sentieon were used to filter out likely artifacts (Sentieon version: v201911). The filtering of somatic variants was performed using QIAGEN Clinical Insight Interpret (version 8.1.20210827; https://digitalinsights.qiagen.com) keeping variants according to the following rules; only non-synonymous and potential splice-site variant (+/– 10bp from exons), minimum 10% variant allele frequency (VAF), total read coverage of >10×, present in gnomAD v2.1.1 (https://gnomad.broadinstitute.org/), 1000 genomes, or the Exome Aggregation Consortium (ExAC) (Cambridge, MA, USA, http://exac.broadinstitute.org) at an allele frequency above <1%. Identification of copy number variants was performed through the Canvas tool [version 1.40.0.1613, Illumina

(21)], while somatic structural variants (SV) and larger indels were called using Manta Structural Variant Caller tool [MantaSV, v1.6.0, Illumina (22)]. The filtering of structural variants was performed according to the following rules; only SVs that were supported by both spanning paired reads (PR) and spanning split reads (SR), and with total supportive reads ≥3 in the tumor sample (T) was retained, and SVs with ≥2 supportive reads in the normal sample (N) were filtered out. All remaining variants were assessed manually using the Integrative Genomics Viewer [IGV, igv.org (23)].

Whole transcriptome sequencing. RNA library was prepared from 100 ng total RNA, using the TruSeq Stranded Total RNA kit with Ribo-Zero Gold, and the Low Sample protocol (15031048 Rev.E, Illumina Inc) according to manufacturer's instruction. The library was sequenced with 2*100 bp pair-end reads using the S1 reagent kit (200 cycles) on NovaSeq 6000 (Illumina). Demultiplexed sequence reads generated 95.7 M read pairs output from the patient RNA sample. RNA sequencing data was analyzed with FusionCatcher v.1.20 (24), using default settings and including the following tools: STAR 2.7.2b, Bowtie v. 1.2.3 and BLAT v.35. The candidate list of potential fusion transcripts was filtered by removing any known false positives ("banned"), transcripts which were out of frame, predicted as intronic, UTR, no-known-CDS, and transcripts with fusion partners containing short repeats, as annotated by FusionCatcher. Reference genome for alignment was GRCh37/hg19 (Feb.2009), alignments were visualized in IGV. RNA-sequencing data was remapped to cDNA sequences of potential fusions and corresponding wild type genes using Bowtie2 (25). RNA-sequencing reads were mapped against all 3 transcripts (fusion and corresponding wild-type transcripts) at a time. The alignments were quality filtered (MAPQ > 20) and any duplicate reads were removed. Supporting spanning reads were counted as unique pairs mapping to a region +/– 5bp from the fusion breakpoint/exon-exon junction.

Reverse transcriptase PCR (RT-PCR) and Sanger sequencing. Total RNA from the first operation, was converted into cDNA using High-Capacity RNA-to-cDNA Kit Applied Biosystems (Thermo Fisher Scientific) according to manufacturer's instruction. Primers targeting the *TPR(4)-ROS(35)* fusion junction and the *TPR* wild type (wt) gene were designed from human genome reference transcripts NM_003292.2 (*TPR*) and NM_002944.2 (*ROS1*) using ExonPrimer (Helmholtz Zentrum, München, Germany). Primers targeting the TPR::ROS1 fusion (forward CTCAACAATCAACTGAAGGCA and reverse CAATCTCCTCTTGGGTTGGA, expected product length=337 bp), and primers targeting the *TPR* wildtype (forward CAACAATCAACTGAAGGCACT and reverse TCAACTCTGTA TTCAGCCATGT, expected product length=350 bp), were ordered from Life Technologies (Carlsbad, CA, USA). PCR was performed on 3 samples [cDNA from tumor, a negative control cDNA, and non-template control (cDNA omitted)], using MyTaq™ DNA Polymerase kit Bioline (Meridian Life Science Inc., Memphis, TN, USA) according to manufacturer's instructions, and run on a Veriti 96 Well Thermal Cycler (Applied Biosystems, Thermo Fisher Scientific). PCR products were inspected using an E-gel® EX 2% agarose using an E-gel® iBase Power system, bands visualized by SYBR Gold (Invitrogen, Thermo Fisher Scientific). The gel was photographed and analyzed with Alpha Imager Mini (v.3.2.2, 2011; Alpha Innotech Corporation, San Leandro, CA, USA). The PCR products were cleaned up with Illustra ExoProStar 1-step according to manufacturer's instruction. Sequencing reaction was performed using BigDye Terminator v3.1 Cycle Sequencing Kit according to manufacturer's instruction. The capillary electrophoresis was performed on an ABI 3500 Genetic Analyzer instrument with POP7 polymer, and sequence results were analyzed in Sequencing Analysis v.6.0 software. All sequencing reagents and protocols were from Applied Biosystems, Thermo Fisher Scientific.

Targeted open-end RNA-sequencing. Anchored Multiplex PCR (AMP™)-based next generation sequencing was performed starting from 250 ng RNA from the first and second operations tumor (FFPE) using the Archer DX FusionPlex Pan Solid Tumor v.2 panel (Invitae Corp., San Francisco, CA, USA), according to manufacturer's instruction. The library was sequenced with 2*151 bp pair-end reads using the Mid Output 2.5 kit (300 cycles) on an Illumina NextSeq 550 instrument. Resulting fastq-files were uploaded and analyzed in Archer Analysis v.6.2. Quality control statistics: 98% of fragments with complete adapter (for both samples), 93% and 95% total fragments on target, fusion QC value was 77.75 and 99.5 (threshold for PASS ≥10), respectively. Using Archer Analysis default settings, strong confidence fusions were filtered for, and only fusions predicted to be in-frame were considered. Detected fusions were manually inspected in JBrowse (jbrowse.org).

DNA methylation profiling. Briefly, DNA from tumor FFPE material from the patient was isolated with the QIAamp® DNA FFPE kit (Qiagen) according to the supplier's instructions with the addition of an extra digestion step with proteinase K overnight. DNA (250-500 ng) was bisulfite-converted with the EZ DNA methylation kit (D5001, Zymo Research, Irvine, CA, USA) and the methylation levels of restored bisulfite-converted DNA was determined with the Infinium Methylation EPIC BeadChip (Illumina) according to the protocols provided by the supplier. Methylation data were processed as previously described (26). Methylation-based classification was performed with the Molecular neuropathology brain classifier version 11b4 (27), and version 12.5 (MNP, www.molecularneuropathology.org/mnp).

Fluorescent in situ hybridization – FISH. FFPE tumor sections (4 μm) were used for interphase FISH analysis of the *ROS1* gene. Paraffin sections were pre-treated in line with procedures recommended by Abbott, Vysis (Vysis Inc., Downers Grove, IL, USA), hybridized with a Zyto*Light*® SPEC ROS1 Dual Color Break Apart Probe (6q22.1) consisting of a 715 kb 3' green probe (chr.6:116,912,298-117,627,255) and a 215 kb 5' orange probe, (chr.6:117,659,135-117,871,701; GRCh37-hg19; ZytoVision GmbH, Bremerhaven, Germany). The tissue slides were counterstained with 4', 6', -diamidino-2'-phenylindole dihydrochloride (DAPI) and photographed using a Zeiss Axioplan 2 Imaging fluorescence microscope. One hundred interphase nuclei were counted by two independent reviewers (×50 nuclei each). The interpretation of intact (wild type/normal), and split signals (fusion gene) was based on accepted international guidelines from the European Cytogeneticists Association.

Transient transfection and western blot. Human embryonic kidney cells (HEK293) were obtained from ATCC Cell Line Collection (Manassas, VA, USA). The cell line was maintained in DMEM supplemented with 10% FBS, 1% L-Glutamine, 1% HEPES solution and 1% sodium pyruvate, at 37˚C with 5% CO2. Three different constructs were generated using the pCMV6-Myc-DDK vector;

pCMV6-ROS1-Myc-DDK ($ROS1^{WT}$), pCMV6-TPR-ROS1-Myc-DDK (TPR-ROS1 fusion) and pCMV6-Myc-DDK (Vector). The wild type ROS1 (NM_002944.2, 2347 aa, #RC221794) and pCMV6 empty vector (#PS10000) constructs were ordered from Origene (Origene, Rockville, MD, USA). Vector construct for the TPR(4)-ROS1(35) fusion transcript (1830 nt) was synthesized, subcloned and sequenced by Invitrogen GeneArt (Thermo Fisher Scientific). HEK293 cells were transfected in 6 well plates (1×10^5 cells/well) with 4 μg of DNA complexed with 10 μl of Lipofectamine 2000 according to the transfection protocol (Invitrogen, Thermo Fisher Scientific). After 48 h from transfection, the cells were harvested, pelleted and protein was extracted by aspirating the media and incubating on ice for 5 min then adding ice cold RIPA buffer (Thermo Fisher Scientific, 89901). Protein lysates (50 μg/sample) were loaded onto Mini-PROTEAN® TGX™ 8-16% gradient gels (BioRad Laboratories, Hercules, CA, USA), protein was blotted onto LF-PVDF membrane (8 min, 25 V and 2.5 A) using a Trans-Blot® Turbo™ Transfer System (BioRad). Blots were subsequently blocked for 1 h at room temperature (RT) in Superblock™ T20 (PBS) blocking buffer as per the manufacturer's recommendations. Altogether, 12 antibodies were used; DDK (DYKDDDDK FLAG® tag, product no. FG4R, Invitrogen, dilution 1:1,000), phosphorylated (p) ROS1 (Tyr2274, product no. PA5-105915, Invitrogen, dilution 1:1,000), total ROS1 (product no. MA5-26760, Invitrogen, dilution 1:2,000), pERK1/2 (Thr202/Tyr204, product no. 4370, Cell Signaling Technology Inc., dilution 1:1,000), total ERK1/2 (product no. 4695, Cell Signaling Technology Inc., dilution 1:1,000), pAKT1/2/3 (Ser 473, product no. sc-514032, Santa Cruz Biotechnology, dilution 1:500), total AKT1 (product no. sc-5298, Santa Cruz Biotechnology, dilution 1:1,000), pSTAT3 (Ser727, product no. 44-384G, Invitrogen, dilution 1:1,000), total STAT3 (product no. MA1-13042, Invitrogen, dilution 1:3,000), S6 (product no. MA5-26760, Invitrogen, dilution 1:2,000), total S6 (product no. 2317S, Cell Signaling Technology Inc., dilution 1:1,000), and GAPDH (product no. 12004168, BioRad, dilution 1:2,500), and they were diluted in PBST (0.1% Tween-20 in PBS). The membranes were incubated overnight at 4˚C with the primary antibodies, after which they were washed 3× 10 min in TBST 0.1% (0.1% Tween-20 in tris-buffered saline). Secondary antibodies; Starbright B520 goat anti-rabbit (12005870, 1:5,000, BioRad), Starbright B700 goat anti-rabbit (12004161, 1:5,000, BioRad) Starbright B700 goat anti-mouse (12004159, 1:5,000, BioRad) and goat anti-mouse Alexa790 (A11357, 1:5,000, Invitrogen) were incubated for 1 h at RT. Transient transfection and Western blot analyses were performed in quadruplicates as four independent experiments. Image detection was performed on ChemiDoc MP (BioRad), and band intensity was quantified using Image lab™ (v. 6.1, BioRad). Protein loading from the different experiments and gels were normalized against total loaded protein from stain free images. The relative phosphorylated to total protein quantities were calculated; pERK/ERK, pAKT/AKT, pSTAT3/STAT3, and pS6/S6. GAPDH was included as visual loading control.

Immunohistochemistry – IHC. Tumor and non-neoplastic FFPE brain tissue sections (4 μm) were mounted on positively charged slides and dried in an oven at 56˚-60˚C for 1 h. Deparaffinization, rehydration and antigen target retrieval were performed with Dako PT100 Link instrument using EnVision FLEX+, High pH (Link) reagents (both from Agilent), according to manufacturer's instruction. Endogenous peroxidases were blocked by EnVision FLEX Peroxidase-Blocking Reagent (Dako) for 5 min incubation at RT. Thereafter, Dako Autostainer (Agilent) was used with an incubation of 60 min at RT with antibodies against ROS1, pSTAT3, pERK, pERK, pAKT. The antibodies were the same as for the Western blot (see above), and dilutions used in the IHC experiments were as follows: 1:1,000 for ROS1, 1:500 for pSTAT3, 1:1,000 for pERK, 1:100 (first operation) and 1:50 (second operation) for pAKT. Tumor tissue with omitted primary antibody was used as negative control. Next, the slides were incubated at RT for 15 min with FLEX+Rabbit (LINKER, Dako K8009) and FLEX+Mouse (LINKER, Dako K8021) followed by a 20 min incubation with FLEX/HRP (Dako K8002) at RT. Diaminobenzidine (DAB) + Chromogen and Mayer's Hematoxylin from the EnVision FLEX kit, was used for staining according to manufacturer's instruction. The IHC slides were digitalized at ×400 magnification with a NanoZoomer S210 (Hamamatsu Photonics, Hamamatsu, Japan). Protein expression of GFAP, ROS1, pSTAT3, pERK, pERK, pAKT was estimated by a semi-quantitative method using ImageJ Fiji according to Crowe and colleagues (28). IHC image deconvolution was performed using the "H DAB" vector, separating the image into hematoxylin staining (image 1) and 3,3'-diaminobenzidine (DAB) staining (image 2). Next, the DAB staining was measured in 4 different areas (450×250 μm, magnification ×400) from each sample/section (corresponding to approximately 450-600 cells from the first operation and 100-300 cells from the second operation per area). The staining intensity was divided by the number of nuclei per image, counted from the hematoxylin image. A mean staining intensity per sample was calculated from the 4 images, and next a fold change between the second and first operation was calculated for each antibody.

Statistical analysis. Normalized Western blot data was presented as a scatter plot of four independent experiments as data points with the mean thereof. Differences were determined by Ordinary one-way ANOVA test followed by Dunnett's multiple comparison test. Calculated significance; $*p<0.05$, $**p<0.01$, $***p<0.001$, $****p<0.0001$. All statistical analyses were conducted using GraphPad Prism version 9.1.1.

Results

Case presentation. This was a previously healthy boy with normal development, who started walking at the age of 13 months. In February 2018, at the age of 16 months, he was referred to the pediatric emergency department due to a progressive deterioration of balance when walking. At examination he was alert but had difficulties maintaining his balance when sitting, and although he could still walk, he lost his balance and fell over after walking 4-5 steps. There was also less movement of his right arm. An acute CT-scan of the brain was performed which showed a 26×28×30 mm hyperdense, rounded tumor in the third ventricle, blocking the interventricular foramen (also known as foramen of Monro), and causing obstructive hydrocephalus. The patient was admitted to hospital and put on corticosteroids. An MRI of the brain and spine confirmed a contrast enhancing rounded tumor in the midline, growing at the roof of the third ventricle, through the left interventricular foramen into the septum pellucidum between the lateral ventricles, causing

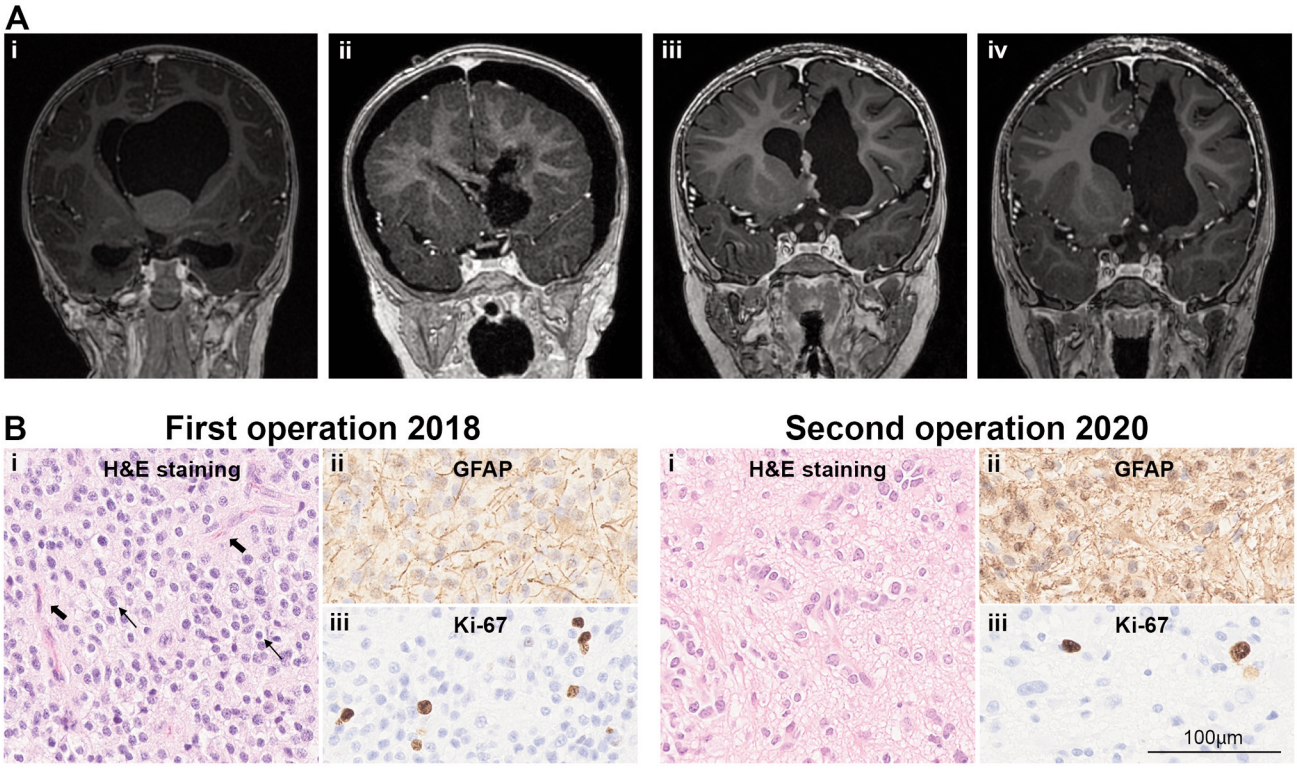

Figure 1. *MR images and histology. A) T1 weighted contrast MR images in coronal plane, (i) at diagnosis March 2018, (ii) after first total resection surgery, (iii) prior to second surgery March 2020, where some tumor tissue can be seen on left side of the septum pellucidum and (iv), 15 months after the second operation, tumor free. B) Histology pictures of formalin fixed paraffin embedded (FFPE) sections areas with high tumor cell content; from the first operation on the left (approximately 95% tumor cell content), and from the second operation on the right (approximately 90-95% tumor cell content). (i) Hematoxylin and eosin staining with tumor cells showing neuroepithelial features. Thin arrows show monomorphic cells, often with clear-cell morphology and round to oval nuclei, and broad arrows show areas with a tendency for pseudorosette formation. (ii) GFAP immunostaining was of varying degree in tumor sections from the first operation, and more heavily stained in tumor sections from the second operation. (iii) Ki-67 proliferation labelling index was up to 10% in sections from the first operation and similar in sections from the second operation. Scale bar represents 100 µm.*

hydrocephalus (Figure 1Ai). There were no signs of metastases in the CNS. Neurosurgery was performed in March 2018; all visible tumor tissue was resected, and a post-operative MRI showed complete resection (Figure 1Aii). The tumor was diagnosed as a low-grade glioma (WHO grade 2). The patient's clinical condition quickly improved, and his balance was largely normalized within two weeks. The boy had MRIs every three months following the operation. Six months post-surgery, a follow up MRI revealed a thin area of contrast enhancing tissue on the left side of the septum pellucidum. Over time, the contrast enhancing tissue very slowly became thicker, indicating a local tumor relapse (Figure 1Aiii). Since the suspected relapse was deemed amenable to local resection, with a good chance of total resection, another surgery was performed two years after the first (March 2020), using intraoperative MRI. Tumor tissue was removed from the left side of the septum pellucidum and medial wall of the left lateral ventricle. No residual tumor tissue was detected by visiual inspection or by MRI. Follow up since then has not shown any signs of relapse, with latest MRI performed 15 months post-operation (Figure 1Aiv). The boy is developing normally.

Clinical routine analyses. Histological examination of the primary tumor from the first operation (2018) revealed a cell-rich neuroepithelial tumor consisting of monomorphic cells, often with clear-cell morphology and round to oval nuclei (Figure 1Bi). Some mitotic figures were noticed (0-2 mitoses/10 HPF). Convincing vascular proliferation or necrotic areas were not seen. Atypical ganglion cells, Rosenthal fibers or eosinophilic granular bodies were not present. In some areas there was a tendency for pseudorosette formation. The border between the tumor and the adjacent parenchyma was diffuse. Immunohistochemistry (IHC) staining showed strong positivity for MAP2, S100, vimentin and Olig2. The neuronal markers NeuN, neurofilament,

Table I. *Methylation profiling results*.

	Classifier v11b4 v3		Classifier v12.5	
Tumor sample	Methylation class - name	Calibrated score	Methylation class - name	Calibrated score
First op. 2018	Infantile hemispheric glioma[b]	0.96911	Paediatric-type diffuse high-grade gliomas[a] MC infant-type hemispheric glioma[c]	0.99826 0.99819
Second op. 2020	No match[d]		No match[d]	

[a]Superfamily; [b]Methylation class; [c]Methylation subclass; [d]Match score limit of ≥0.9.

synaptophysin and chromogranin were negative. Tumor cells were also negative for TTF1, EMA, CD34, whereas ATRX and H3K27me3 were retained. Glial fibrillary acidic protein (GFAP) was weakly positive, and mean Ki-67/MIB-1 proliferation index was 4.2% (2.5-5.8%) in the primary tumor (Figure 1Bii and iii). The fraction of neoplastic cells was estimated to be 90% in the whole section of the primary tumor. Routine clinical molecular analysis revealed the tumor to be negative for the four most common *KIAA1549::BRAF* fusions, as well as *BRAF*-, *IDH1*-, *IDH2*- and H3K27M mutations. The tumor was initially considered to be a low-grade glioma (WHO grade 2, 2016) but was, after evaluation at a reference center, classified as a densely cellular glial tumor compatible with pilocytic astrocytoma (WHO grade 1, 2016) with increased mitotic and proliferative activity. Four months after the first diagnosis, methylation analysis was performed and classified the tumor as an infant-type hemispheric glioma (classifier v11b4, German Cancer Research Center (DKFZ), Heidelberg, Germany). Later on, the updated classifier version v12.5 was run, and showed the same result (Table I). Histological examination of the tumor from the second operation (2020) showed a 2-fold stronger positive GFAP staining compared to the first operation (Figure 1Bii). However, the mean Ki-67/MIB-1 proliferation index was not higher in sections from the second operation (mean of 3.1% compared to 4.2%), and in both operations hot-spot regions with up to 10% positive cells could be seen (Figure 1Biii). The fraction of neoplastic cells was estimated to be 70% in the whole section, and the methylation array failed to classify the tumor from the second operation (neither v11b4 nor v12.5), probably due to an insufficient content of neoplastic cells.

Molecular analyses. Paired whole genome sequencing (WGS) of the primary tumor (first operation) revealed one somatic non-synonymous variant of unknown clinical significance, 7 structural variants (SVs), and several copy-number changes (Table II). Ploidy for the whole tumor genome was estimated to near diploid (1.94), and tumor purity was 82% according to the Canvas tool. The main segmental gains and losses were located in chromosome 1, 2, 6, 8, causing breakpoints within 10 genes (Figure 2A; Table II). Complementary whole transcriptome sequencing (RNA-sequencing) and analysis by FusionCatcher identified two potential in-frame fusion transcripts, matching the structural variants identified in the WGS data; *TPR(4)::ROS1(35)* (chr. 1q31.1 and chr.6q22.1) and *ING5(7)::NFKBIE(2)* (chr. 2q37.1 and chr. 6p21.1). By remapping the transcriptome data to cDNA sequences of the fusion genes and corresponding wild type (wt) genes, we could correctly quantify the number of supportive spanning reads (Table III). The *ING5::NFKBIE* fusion transcript was expressed to a lower extent than its corresponding wild type transcripts [11 supportive spanning reads compared to 17 (*ING5*) and 16 (*NFKBIE*) wt]. The *TPR::ROS1* fusion was highly expressed (17 supportive spanning reads), and while the *TPR* wild type gene showed higher expression (29 supportive reads) there were no supporting reads corresponding to the *ROS1* wild type transcript (Figure 2D; Table III). Viewing the transcriptomic breakpoints in Integrative Genomics Viewer (IGV) showed only the 3' end of the *ROS1* transcript to be expressed (from exon 35 and onwards; Figure 2B). Hence, we concluded that all *ROS1*-reads were originating from the fusion transcript, and no wild type *ROS1* was expressed in the tumor tissue. While *ROS1* fusion genes are well-known oncogenic drivers (29, 30), both *ING5* and *NFKBIE* are mainly reported in cancer context as tumor suppressor genes (31, 32), directing our attention to the *TPR::ROS1* fusion gene for further analysis. The junction between *TPR* and *ROS1* was verified by reverse transcription PCR (RT-PCR) based Sanger sequencing, leading to a fusion protein of 625 amino acids with a retained tyrosine kinase domain from *ROS1* (Figure 2C). Also, interphase fluorescent *in situ* hybridization (FISH) using break apart probes for *ROS1* confirmed that *ROS1* is involved in a fusion rearrangement in tumor cells (Figure 2E).

After receiving new tumor tissue from the second operation, we performed targeted open-end RNA-sequencing (FusionPlex) to verify the *TPR::ROS1* fusion gene. We found 27 unique reads (representing 93% of reads) spanning the *TPR(4)::ROS1(35)* breakpoint (Table IV). In addition, the

Table II. *Somatic variants called from WGS data.*

Variant type[a]		Position[b]	Genes involved[c]	Coding variant[d]	VAF (%) or Ploidy[e]
SNV	missense	chr17:3844897	ATP2A3	c.1597C>T, p.R533C	43%
SV	bnd	chr1:62595194; chr6:43179782	in:PATJ; in:CUL9	NRG1(1)::CUL9(27)	22%
	bnd	chr1:62596860;chr8:32074899	in:PATJ; in:NRG1	NRG1(1)::CUL9(27)	22%
	dup	chr1:67095761;chr1:155201558	in:SGIP1;GBAP1		28%
	bnd	chr1:186,336,971,chr6:117643131	in:TPR; in:ROS1	TPR(4)::ROS1(35)	31%
	bnd	chr1:190389925;chr2:233649235	in:BRINP3; in:GIGYF2		32%
	bnd	chr2:27024117;chr8:123867008	CENPA; in:ZHX2		24%
	bnd	chr2:242663225;chr6:44231807	in:ING5; in:NFKBIE	ING5(7)::NFKBIE(2)	20%
CNV	loss	chr1:pter-67,1mb	in:SGIP1	1p-del	1
	loss	chr1:155,2-186,3mb	in:TPR	interstitial 1q-del	1
	loss	chr1:190,4mb-qter	in:BRINP3	1q-del	1
	loss	chr2:pter-27mb		2p-del	1
	gain	chr2:233,6-242,7mb	in:GIGYF2; in:ING5	interstitial 2q-gain	3
	gain	chr6:43,2-44,2mb	in:CUL9, TTBK1, CRIP3, ZNF318, ABCC10, TJAP1, POLR1C, POLH, RSPH9, VEGFA, LINC02537, LINC01512, NR_125865.1, MRPL14, CAPN11, MYMX, SLC29A1, HSP90AB1, SLC35B2, in:NFKBIE	interstitial 6p-gain (1020kb)	3
	loss	chr6:117,6mb-qter	in:ROS1	6q-del	1
	gain	chr8:pter-32,1mb	in:NRG1	8p-gain	3
	gain	chr8:123,9mb-qter	in: ZHX2	8q-gain	1

[a]Single nucleotide variants (SNV), structural variants (SV), and copy number variants (CNV) were called by TNscope, MantaSV, and Canvas, respectively. Missense: amino acid exchange; bnd: adjacent break ends resulting in translocation or inversion; dup: duplication; loss: loss of material from genomic region; gain: gain of material from genomic region. [b]Position according to Hg19 [GRCh37]; chr: chromosome; mb: megabases; kb: kilobases. [c]Gene symbol of genes affected by the variant, "in:" means that the breakpoint is located within the gene (intron or exon), gene accession numbers as follows: ATP2A3 (NM_174953.3), NRG1 (NM_013962.3), CUL9 (NM_015089.4), ROS1 (NM_002944.2), TPR (NM_003292.2), ING5 (NM_032329.6), NFKBIE (NM_004556.3). [d]Variant effect on genome, cDNA (c) and protein (p) change according to HGVS nomenclature. Brackets indicate exon boundaries involved in the fusion junction. [e]VAF: Variant allele frequency (%) of reads from alternative allele divided by the total number of reads in the region. For SV the alternative allele frequency was calculated from the sum of paired read (PR) and split read (SR) coverage. Ploidy (copy number state) is presented for CNV variants. The impact of the ATP2A3 c.1597C>T, p.R533C variant was predicted from the following information: Predicted as: Damaging (SIFT), benign (PolyPhen-2), present in gnomAD (frequency:0.002), listed in COSMIC (ID:8044088), and dbSNP (ID:772480917) databases.

FusionPlex analysis also revealed a *NRG1(1)::CUL9(27)* fusion of unknown function (25 unique reads representing 32% of reads spanning the breakpoint). The breakpoints, intron 1 in *NRG1* and intron 26 in *CUL9*, matched the DNA breakpoints found by WGS/Manta in the primary tumor, and the fusion seemed to arise through a complex rearrangement between chr. 1, 6 and 8 (Table II). However, neither targeted FusionPlex RNA-sequencing nor whole transcriptome sequencing of the primary tumor (first operation), found any evidence for the *NRG1::CUL9* fusion (no supportive reads), probably due to its low expression. Moreover, the fusion part of *NRG1* (exon1) corresponds to the 5' UTR region (before the ATG start site); hence it is unclear if this fusion leads to a translated and functional protein.

Functional analyses. As *ROS1* is known to be involved in oncogenic fusion genes and since targeted therapies have been developed for *ROS1* driven tumors, we proceeded to investigate the functional consequence of the *TPR::ROS1* fusion gene found in this case. HEK293 cells were transiently transfected by three pCMV6 cDNA constructs; *TPR(4)*::*ROS1(35)* fusion (TPR::ROS1), *ROS1* wild type ($ROS1^{WT}$), and empty pCMV6 vector (Vector). Western blot using DDK antibodies (targeting the FLAG Tag) on protein lysates from the transfected cells, confirmed the expression of the constructs (a ROS1-DDK band at 200 kDa and a TPR::ROS1-DDK at 130 kDa; Figure 3A). Four independent experiments with antibodies targeting ROS1, ERK, AKT, STAT, S6 and their corresponding active (phosphorylated)

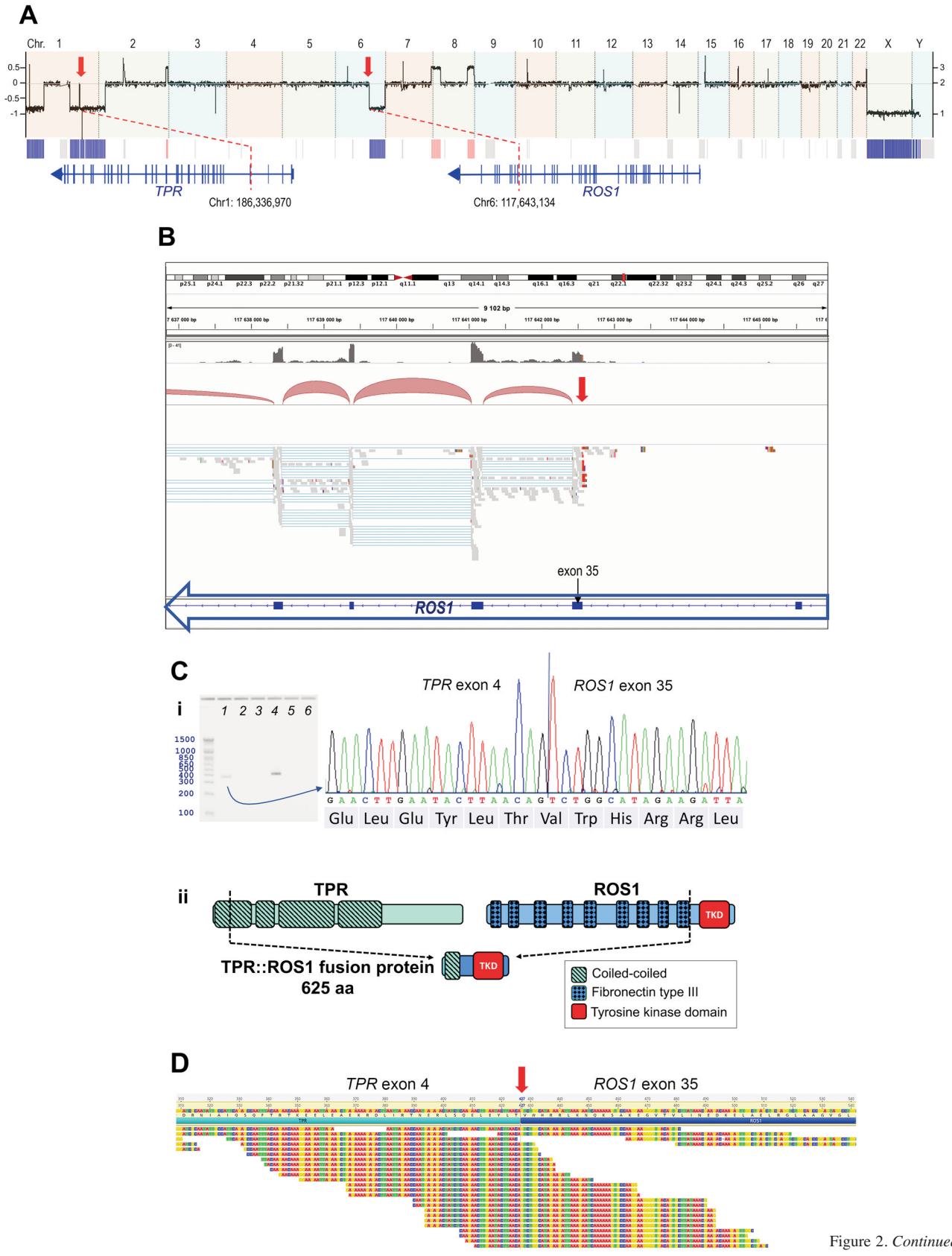

Figure 2. *Continued*

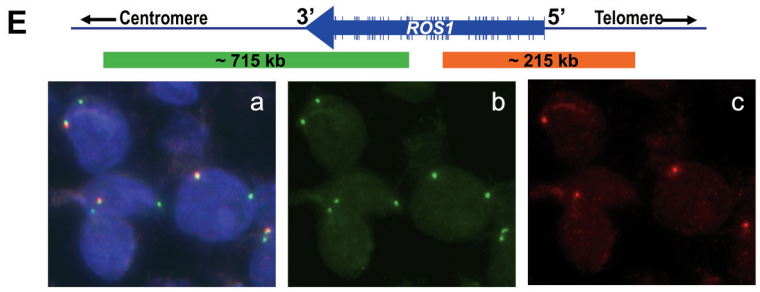

Figure 2. *Molecular analyses. A) Copy number profile from WGS data from the primary tumor visualized in Integrative Genomics Viewer (IGV), where two segmental losses in chr. 1q22-q31.1 and 6q22.1-qter (red arrows) result in breakpoints in the TPR gene (left) and the ROS1 gene (right). The y-axis shows logarithmic value (log2) of normalized coverage from Canvas (left), and ploidy/copy number state (right). B) RNA-sequencing data visualized in IGV showing ROS1 expression to start at exon 35 and onwards (expression from exon 1-34 are missing). Genomic positions are according to Hg19 (GRCh37). C) RT-PCR and Sanger sequencing of cDNA from the fusion transcript. (i) PCR- products on agarose gel (left) showing a 337 bp fragment band of the TPR::ROS1 fusion (lane no. 1), and a 350 bp fragment band of the TPR wild type (lane no. 4) as expected, and run with negative control cDNA (lane no. 2 and 5) and non-template control (NTC, lane no. 3 and 6) for each PCR reaction, respectively. Sequencing electropherogram (right) of the TPR::ROS1 fusion PCR product showing a junction between TPR exon 4 at position c.427 (NM_003292.2) and ROS1 exon 35 at position c.5642 (NM_002944.2). Amino acid (aa) sequence is shown underneath the electropherogram. (ii) Schematic presentation of native TPR protein (2363 aa; NP_003283.2 and ROS1 (2347 aa; NP_002935.2) with the breakpoint position in TPR (at aa 142) and ROS1 (at aa 1881, dotted line) generate a putative fusion protein of 625 aa, containing one coiled-coil domain from TPR joined to the tyrosine kinase domain of ROS1. Domains and positions are according to UniProtKB (http://uniprot.org). D) Spanning reads after remapping of transcriptomic sequencing data from the primary tumor to the cDNA sequence of the TPR::ROS1 fusion gene (NM_003292.2; NM_002944.2). E) Interphase FISH on primary tumor tissue using a ROS1 Dual Colour Break Apart Probe, consisting of a 715 kb 3' green probe and a 215 kb 5' orange probe at the 6q22.1 locus (not to scale). Tumor cells display a wild type allele with a merged green/red (yellow) signal and a lone green signal representing the retained 3'-end of the TPR::ROS1 fusion, according to the Merged (left), ZyOrange (middle), and ZyGreen channel (right) of the photo.*

Table III. *Remapping of whole transcriptome sequencing data to cDNA transcripts.*

Transcript	Nt position at breakpoint[a]	Transcript accession no.	# Spanning reads[b]
TPR::ROS1 fusion	427	NM_003292.2-NM_002944.2	17
ROS1 wt	5641	NM_002944.2	0
TPR wt	427	NM_003292.2	29
ING5::NFKBIE fusion	680	NM_032329.6-NM_004556.3	11
ING5 wt	680	NM_032329.6	17
NFKBIE wt	365	NM_004556.3	16

Whole transcriptome (RNA-sequencing) data from the first operation. [a]Nt (nucleotide) position at breakpoint (exon-exon junction) from ATG start site. [b]Number of unique spanning reads overlapping the breakpoint at least 5bp (spanning reads from pairs are only calculated once).

forms were analyzed to explore the downstream effect of the MAPK-, PI3K- and JAK/STAT-signaling pathways. Western blot analysis of the TPR::ROS1 fusion gene constructs showed a significant 3.5-fold ($p<0.01$) upregulation of phosphorylated (p) ROS1/total ROS1, a 6.1-fold ($p<0.001$) upregulation of pERK/total ERK, a 2.1-fold ($p<0.001$) upregulation of pAKT/total AKT, a 2.4-fold ($p<0.01$) upregulation of pSTAT3/total STAT3, and a substantial 9.0-fold ($p<0.0001$) upregulation of pS6/total S6 as compared to the *ROS1*^{WT} gene constructs (Figure 3A). Moreover, the activation of the, MAPK-, PI3K- and JAK/STAT-pathways was confirmed in primary tumor FFPE sections from the first and second operation by immunohistochemistry of pSTAT3, pAKT and pERK (Figure 3B). Overall, a strong immunostaining was observed in tumor cells from both the first and second operation for all proteins, as compared to non-neoplastic brain control tissue. However, protein expression of ROS1 and pSTAT3 was also present in normal tumor brain tissue. Tumor cells showed cytoplasmic immunopositivity for ROS1, while pSTAT3, pAKT and pERK mainly showed nuclear immunostaining. Phosphorylated ERK displayed the strongest expression, both nuclear and to a lesser extent cytoplasmic, of all phosphorylated proteins. Comparing the samples from first and second operation, the relapsed tumor sample showed a stronger staining intensity for pSTAT3 (2-fold), pAKT (4-fold) and pERK (2-fold; Figure 3B). However, these results should be interpreted with caution as IHC is not a fully quantitative method and there are too few

Table IV. *Targeted RNA sequencing results, FusionPlex panel.*

Sample	Gene fusion	No. reads[a]	% of reads[b]	Breakpoint[c]
First op. 2018	*TPR::ROS1*	26	96.30	chr1:186337018, chr6:117642557
Second op. 2020	*TPR::ROS1*	27	93.10	chr1:186337018, chr6:117642557
	NRG1::CUL9	25	32.05	chr8:31498245, chr6:43180887

[a]Number of unique reads supporting the fusion. [b]The percent of reads supporting the fusion (number of unique reads spanning the breakpoints divided by the total number of unique reads that span either breakpoint). [c]Breakpoints of the fusion genes, in hg19 [GRCh37] coordinates.

samples (n=2) to calculate significance. Also, there are many factors that can affect the staining intensity in different tissue preparations.

Discussion

In this study, we analyzed the tumor tissue of a now 5-year-old boy, diagnosed with a midline low-grade glioma and having undergone two total resection surgeries within 2 years. A novel *TPR(4)::ROS1(35)* fusion gene was identified, which was further shown to activate the MAPK-, PI3K- and JAK/STAT- pathways by functional *in vitro* analyses.

The nucleoprotein TPR, encoded by the *TPR* gene, is part of the nuclear pore complexes which are involved in exporting both RNA and proteins from the nucleus of the cell (33). TPR contains coiled-coil domains that are retained in the 5' end of all *TPR* fusion variants reported to date (34-40). ROS1 fusion partners with coiled-coil domains are also frequently found in non-small-cell lung cancer (NSCLC) (*e.g.*, *EZR::ROS1*, *TPM3::ROS1*, *CCDC6::ROS1*) and are thought to be responsible for the activation of the tyrosine kinase domain of the 3' fusion partner through homodimerization (41, 42). For example, the 5' PML partner in a PAX5::PML fusion in a pediatric acute lymphocytic leukemia patient, was functionally demonstrated to mediate dimerization through the coiled-coil by *in vitro* studies (43). *TPR* fusions has previously been reported in a few pediatric cancers including *TPR::NTRK1* in a high-grade undifferentiated sarcoma (44), a mesenchymal tumor of the small intestine (45), and in a mesenchymal tumor of the neck region (36), a *TPR::RET* fusion detected in a papillary thyroid carcinoma (46), a *TPR::ROS1* fusion detected in lipofibromatosis (37). Also, a *TPR::ROS1* fusion was recently reported in an adult lung adenocarcinoma case (47).

The *ROS1* gene encodes a proto-oncogene 1 tyrosine-protein kinase which is part of the sevenless subfamily of tyrosine kinase insulin receptor genes. It has structural similarity to the anaplastic lymphoma kinase (ALK) protein; approximately 50% homology overall, and 75% homology at the ATP binding site (30). In adults, ROS1 is mainly expressed in testis (epididymis) and lung (alveolar cells), and shows some expression in the brain (cerebellar cortex; https://www.proteinatlas.org/ENSG00000047936-ROS1/tissue), while the main subcellular location of ROS is in cytoplasmic vesicles (48). The ligand(s) of ROS are still unknown in humans, however in mice the ligand neural epidermal growth factor-like like 2 (NELL2) has been identified (29). Activated ROS1 stimulates further autophosphorylation recruiting adaptor proteins, in turn bringing on a cascade of signals via MAPK-, PI3K and JAK-pathways (49). In this study, we found the activation of these three pathways to be significantly elevated in cells carrying the novel TPR::ROS fusion protein by *in vitro* studies of HEK293 cells. Also, expression of phosphorylated downstream mediators was markedly present in tumor tissue sections from the patient, with pERK showing the strongest staining in both the primary and relapsed tumor. The most elevated activation by phosphorylation in *TPR::ROS1*-fusion-transfected-cells was seen for the downstream mediator S6 (rpS6 or eS6), which probably is due to its mutual activation of both the MAPK- and the PI3K-pathways (50). The S6 protein is a component of the 40S ribosomal subunit and has multiple functions in the cell, including ribosome biogenesis, regulation of the cell-cycle and tumorigenesis (51).

Oncogenic *ROS1* fusion genes in various cancers are mostly due to chromosomal rearrangement (37, 52, 53). *ROS1* fusions are most commonly detected in NSCLC, where the most frequent types are *CD74::ROS1*, *EZR::ROS1*, *SDC4::ROS1* and *SLC34A2::ROS1* (54). Overall, more than 55 different *ROS1* fusion genes with various 5' partners have been detected in different cancer forms, with the frequency of individual fusion partners varying between tumor types (29). In pediatric glioma, *GOPC::ROS1*, *CEP85L::ROS1* and *KLC1::ROS1* fusions have been reported, and similar to the *TPR::ROS1* fusion identified in the present study they show retained exon 35-43 of *ROS1*, leading to intact, released and upregulated tyrosine kinase domain (55, 56).

By histopathological examination of the primary tumor, the current case was diagnosed as a low-grade glioma (WHO grade 1) with increased mitotic and proliferative activity, and methylation profiling classified it as an

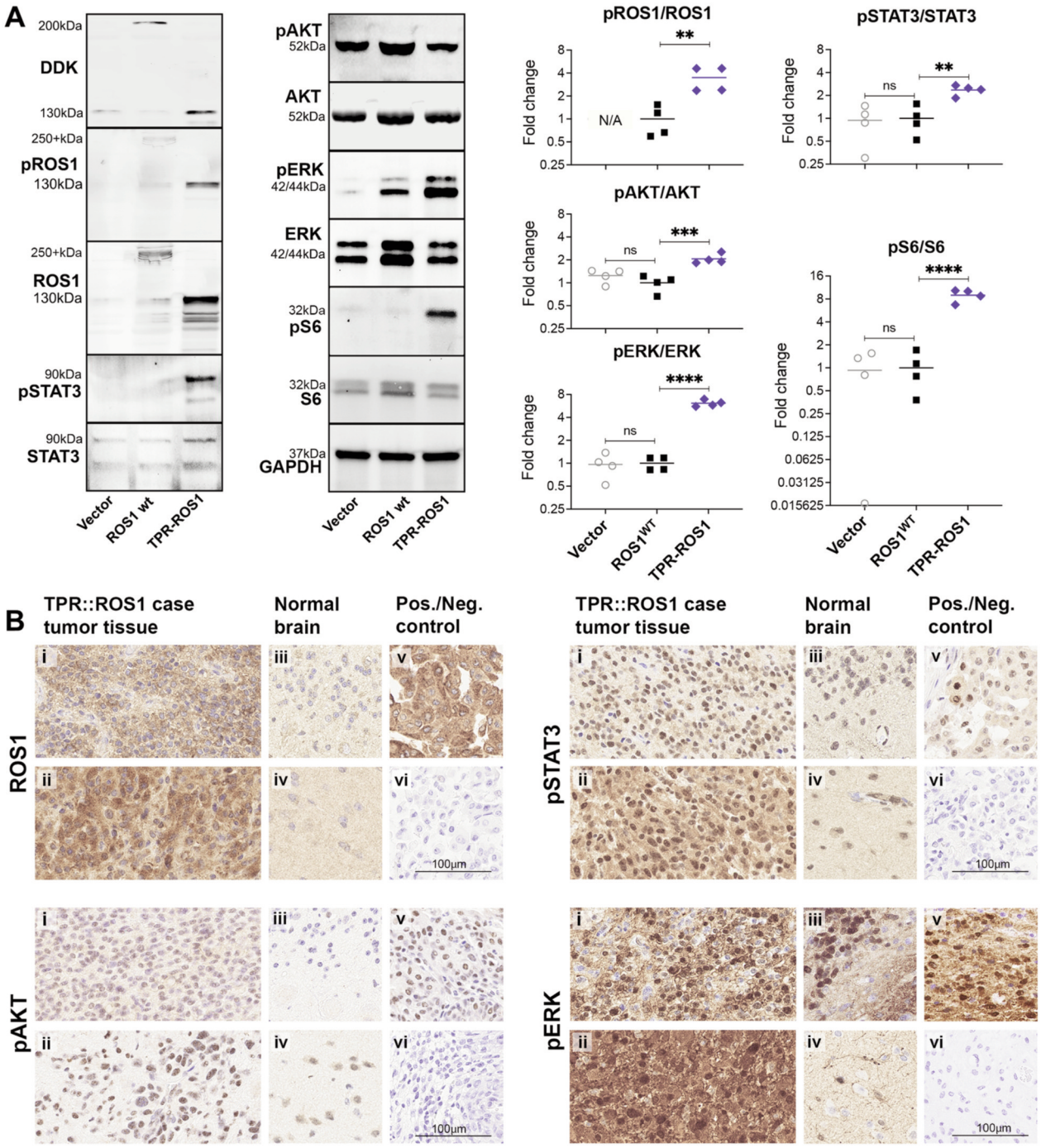

Figure 3. *Functional analyses with Western blot and IHC. A) Western Blot imaging (left) of HEK293 transiently transfected constructs: empty vector (Vector), ROS1 wild type (ROS1^{WT}) and fusion gene (TPR::ROS1), probed with antibodies against DDK (TPR::ROS1-DDK at 130 kDa and ROS1-DDK at 200+ kDa), Phosphorylated (p) ROS1-Tyr2274 (130 kDa for TPR::ROS1; 200+ kDa for ROS1^{WT}), total ROS1 (130 kDa for TPR::ROS1; 200+ kDa for ROS1^{WT}), pSTAT3-Ser272 (90 kDa), total STAT3 (90 kDa), pAKT-1/2/3 (52 kDa), total AKT (52 kDa), pERK-Thr202/Tyr204 (44/42 kDa), total ERK (44/42 kDa), pS6-Ser235/236 (32 kDa), total S6 (32 kDa), and GAPDH (37 kDa). Blots show representative bands from one out of four independent experiments. Scatter plot (right) shows ratio pSTAT3/STAT3, pERK/ERK, pAKT/AKT and pS6/S6 protein quantity from four experiments, calculated as fold change (FC) compared to the mean of ROS1^{WT}. Significance; *p<0.05, **p<0.01, ***p<0.001, ****p<0.0001, ns: not significant. B) IHC of FFPE sections from the TPR::ROS1 case and normal controls stained with ROS1, pSTAT3, pAKT and pERK antibodies. (i) Tumor tissue from first operation, (ii) tumor tissue from second operation, (iii) normal cerebellum, (iv) normal cortex tissue (from the second operation). (v) Positive and (vi) negative control tissues were as follows; ROS1 fusion positive lung adenocarcinoma (for ROS1 and pSTAT3 staining), normal urothelial tissue (for pAKT staining), and BRAF fusion positive pilocytic astrocytoma (for pERK staining). Negative controls had no primary antibody. Original magnification ×400. Scale bar represents 100 µm.*

infantile hemispheric glioma. At that time point, "infantile hemispheric glioma" was not a defined subtype by WHO (3). In 2019, Guerreiro Stucklin *et al*. published a retrospective study of infant gliomas, and identified three clinical groups; 1) hemispheric glioma characterized by genetic alterations in *ALK*, *MET*, *NTRK* and *ROS1*, 2) hemispheric glioma characterized by RAS/MAPK activation, and 3) midline glioma characterized by RAS/MAPK activation (16). The vast majority of group 1 tumors were HGG, and they were almost exclusively hemispheric tumors. The survival of group 1 tumors was heterogeneous. The *ROS1* fused tumors, comprising about a third of group 1 (7 cases), had a five-year overall survival of approximately 25%. The current case was a midline pLGG with *ROS1* fusion, and hence is not fully consistent with the group 1 category described by Guerreiro Stucklin *et al*. However, the authors propose that group 1 tumors may comprise a spectrum of LGG/HGG with the potential to transform in both directions. Moreover, young children with LGG are reported to have worse survival when compared with older children, and the opposite is suggested for HGG, indicating that the tumor grading may not be very decisive for pediatric glioma (16, 57). The methylation class of infantile hemispheric glioma includes tumors with a broad morphological spectrum, often with a higher grade, that are histologically more akin to glioblastoma or anaplastic astrocytoma (58). In the most recent WHO classification of CNS tumors, 2021 (18), infant-type hemispheric glioma is now included as a separate type in the pediatric-type diffuse high-grade glioma group. According to the WHO classification of CNS tumors, these gliomas appear as large masses in the supratentorial compartment with frequent superficial involvement (59), which is in contrast with the tumor of the current case which was located in the interventricular foramen area. However, since the reported number of ROS-driven pLGG/pHGG cases are still very few (5, 60), it is difficult to draw any major conclusions regarding location, staging, survival probability and progression of these tumor types.

ROS fusions are emerging as clinically important since they can be targeted by small inhibitors. Hence, it is becoming crucial to identify ROS-driven tumors by genetic screening so that the patients may benefit from these treatments (5, 14, 47, 60-63). Several ROS inhibitors that have been developed are mainly tested for adult patients with NSCLC (64). Currently, three are being evaluated for children; ensartinib, entrectinib and repotrectinib (clinical open trials: Ensartinib NCT03213652 phase II, Entrectinib NCT02650401phase I/II, Repotrectinib NCT04094610 phase I/II) (29, 60, 65-68). Hopefully these trials will lead to ROS-inhibitors approved for clinical use for children with brain tumors and could help the current patient in case of relapse.

Conclusion

A novel *TPR::ROS1* fusion gene was identified in a recurrent case of pediatric low-grade glioma, classified as infantile hemispheric glioma by methylation profiling. The *TPR::ROS1* fusion was shown to activate the downstream oncogenic pathways MAPK, PI3K and JAK/STAT. The diagnostic evolution of pediatric CNS tumors is still emerging. This case report adds to the complexity of subtype division and broadens the knowledge of new fusion genes and subtype characteristics. Ongoing clinical trials with targeted therapy for ROS-driven tumors will hopefully generate new treatment possibilities for children with these rearrangements.

Conflicts of Interest

The Authors declare no potential conflicts of interest.

Authors' Contributions

FA and MS initiated the study. FA supervised the study. LD and FA drafted the manuscript. MS provided the clinical information, MRI images and informed consent from the patient's parents. LD performed RT-PCR, Sanger sequencing, and targeted RNA-sequencing. FA conducted whole genome sequencing data filtering and interpretation. SK performed the in vitro transfections and Western blot experiments, supervised by KE. TOB and HF analyzed and interpreted the histopathological and immunohistochemistry tumor sections. AEL performed bioinformatic analysis of the whole transcriptome RNA sequencing. HS performed the FISH experiments. HC performed methylation profiling. MT provided tumor samples from surgery. JAN supervised the immunohistochemistry experiments. All authors read and approved the manuscript.

Acknowledgements

We would first of all like to thank the patient and his family for the participation in this study. We thank Carina Karlsson for performing immunohistochemical experiments. The whole genome sequencing and whole transcriptome sequencing were run at the Center for Medical Genomics (CMG) at the Department of Clinical Genetics and Genomics, Sahlgrenska University Hospital, Gothenburg, Sweden. Bioinformatic analysis of whole genome sequencing was performed at the SciLife Clinical Genomics Gothenburg unit. This work was supported by the Swedish Cancer Society (www.cancerfonden.se, grant number 2018/825 to FA and grant number 2018/652 to JAN), the Swedish Children's Cancer Foundation (www.barncancerfonden.se, grant number PR2017-0029 to FA, PR2019-0079 to KE, and KP2019-0010 to HC), and the ALF-agreement (www.researchweb.org/is/alfgbg, ALFGBG-716231 to FA, ALFGBG-965828 to HC, and ALFGBG-719301 to JAN).

References

1 Lannering B, Sandström PE, Holm S, Lundgren J, Pfeifer S, Samuelsson U, Strömberg B, Gustafsson G and Swedish Childhood CNS Tumor Working Group (VCTB): Classification, incidence and survival analyses of children with CNS tumours

diagnosed in Sweden 1984-2005. Acta Paediatr *98(10)*: 1620-1627, 2009. PMID: 19594464. DOI: 10.1111/j.1651-2227.2009.01417.x

2 Ostrom QT, Cioffi G, Gittleman H, Patil N, Waite K, Kruchko C and Barnholtz-Sloan JS: CBTRUS Statistical Report: Primary brain and other central nervous system tumors diagnosed in the United States in 2012-2016. Neuro Oncol *21(Suppl 5)*: v1-v100, 2019. PMID: 31675094. DOI: 10.1093/neuonc/noz150

3 Louis DN, Perry A, Reifenberger G, von Deimling A, Figarella-Branger D, Cavenee WK, Ohgaki H, Wiestler OD, Kleihues P and Ellison DW: The 2016 World Health Organization classification of tumors of the central nervous system: a summary. Acta Neuropathol *131(6)*: 803-820, 2016. PMID: 27157931. DOI: 10.1007/s00401-016-1545-1

4 Armstrong GT, Liu Q, Yasui Y, Huang S, Ness KK, Leisenring W, Hudson MM, Donaldson SS, King AA, Stovall M, Krull KR, Robison LL and Packer RJ: Long-term outcomes among adult survivors of childhood central nervous system malignancies in the Childhood Cancer Survivor Study. J Natl Cancer Inst *101(13)*: 946-958, 2009. PMID: 19535780. DOI: 10.1093/jnci/djp148

5 Ryall S, Tabori U and Hawkins C: Pediatric low-grade glioma in the era of molecular diagnostics. Acta Neuropathol Commun *8(1)*: 30, 2020. PMID: 32164789. DOI: 10.1186/s40478-020-00902-z

6 Jones DT, Kocialkowski S, Liu L, Pearson DM, Bäcklund LM, Ichimura K and Collins VP: Tandem duplication producing a novel oncogenic BRAF fusion gene defines the majority of pilocytic astrocytomas. Cancer Res *68(21)*: 8673-8677, 2008. PMID: 18974108. DOI: 10.1158/0008-5472.CAN-08-2097

7 Tomić TT, Olausson J, Wilzén A, Sabel M, Truvé K, Sjögren H, Dósa S, Tisell M, Lannering B, Enlund F, Martinsson T, Åman P and Abel F: A new GTF2I-BRAF fusion mediating MAPK pathway activation in pilocytic astrocytoma. PLoS One *12(4)*: e0175638, 2017. PMID: 28448514. DOI: 10.1371/journal.pone.0175638

8 Schindler G, Capper D, Meyer J, Janzarik W, Omran H, Herold-Mende C, Schmieder K, Wesseling P, Mawrin C, Hasselblatt M, Louis DN, Korshunov A, Pfister S, Hartmann C, Paulus W, Reifenberger G and von Deimling A: Analysis of BRAF V600E mutation in 1,320 nervous system tumors reveals high mutation frequencies in pleomorphic xanthoastrocytoma, ganglioglioma and extra-cerebellar pilocytic astrocytoma. Acta Neuropathol *121(3)*: 397-405, 2011. PMID: 21274720. DOI: 10.1007/s00401-011-0802-6

9 Bale TA: FGFR- gene family alterations in low-grade neuroepithelial tumors. Acta Neuropathol Commun *8(1)*: 21, 2020. PMID: 32085805. DOI: 10.1186/s40478-020-00898-6

10 Ardizzone A, Scuderi SA, Giuffrida D, Colarossi C, Puglisi C, Campolo M, Cuzzocrea S, Esposito E and Paterniti I: Role of fibroblast growth factors receptors (FGFRs) in brain tumors, focus on astrocytoma and glioblastoma. Cancers (Basel) *12(12)*: 3825, 2020. PMID: 33352931. DOI: 10.3390/cancers12123825

11 Jain P, Fierst TM, Han HJ, Smith TE, Vakil A, Storm PB, Resnick AC and Waanders AJ: CRAF gene fusions in pediatric low-grade gliomas define a distinct drug response based on dimerization profiles. Oncogene *36(45)*: 6348-6358, 2017. PMID: 28806393. DOI: 10.1038/onc.2017.276

12 Bandopadhayay P, Ramkissoon LA, Jain P, Bergthold G, Wala J, Zeid R, Schumacher SE, Urbanski L, O'Rourke R, Gibson WJ, Pelton K, Ramkissoon SH, Han HJ, Zhu Y, Choudhari N, Silva A, Boucher K, Henn RE, Kang YJ, Knoff D, Paolella BR, Gladden-Young A, Varlet P, Pages M, Horowitz PM, Federation A, Malkin H, Tracy AA, Seepo S, Ducar M, Van Hummelen P, Santi M, Buccoliero AM, Scagnet M, Bowers DC, Giannini C, Puget S, Hawkins C, Tabori U, Klekner A, Bognar L, Burger PC, Eberhart C, Rodriguez FJ, Hill DA, Mueller S, Haas-Kogan DA, Phillips JJ, Santagata S, Stiles CD, Bradner JE, Jabado N, Goren A, Grill J, Ligon AH, Goumnerova L, Waanders AJ, Storm PB, Kieran MW, Ligon KL, Beroukhim R and Resnick AC: MYB-QKI rearrangements in angiocentric glioma drive tumorigenicity through a tripartite mechanism. Nat Genet *48(3)*: 273-282, 2016. PMID: 26829751. DOI: 10.1038/ng.3500

13 Ramkissoon LA, Horowitz PM, Craig JM, Ramkissoon SH, Rich BE, Schumacher SE, McKenna A, Lawrence MS, Bergthold G, Brastianos PK, Tabak B, Ducar MD, Van Hummelen P, MacConaill LE, Pouissant-Young T, Cho YJ, Taha H, Mahmoud M, Bowers DC, Margraf L, Tabori U, Hawkins C, Packer RJ, Hill DA, Pomeroy SL, Eberhart CG, Dunn IF, Goumnerova L, Getz G, Chan JA, Santagata S, Hahn WC, Stiles CD, Ligon AH, Kieran MW, Beroukhim R and Ligon KL: Genomic analysis of diffuse pediatric low-grade gliomas identifies recurrent oncogenic truncating rearrangements in the transcription factor MYBL1. Proc Natl Acad Sci USA *110(20)*: 8188-8193, 2013. PMID: 23633565. DOI: 10.1073/pnas.1300252110

14 Zhang J, Wu G, Miller CP, Tatevossian RG, Dalton JD, Tang B, Orisme W, Punchihewa C, Parker M, Qaddoumi I, Boop FA, Lu C, Kandoth C, Ding L, Lee R, Huether R, Chen X, Hedlund E, Nagahawatte P, Rusch M, Boggs K, Cheng J, Becksfort J, Ma J, Song G, Li Y, Wei L, Wang J, Shurtleff S, Easton J, Zhao D, Fulton RS, Fulton LL, Dooling DJ, Vadodaria B, Mulder HL, Tang C, Ochoa K, Mullighan CG, Gajjar A, Kriwacki R, Sheer D, Gilbertson RJ, Mardis ER, Wilson RK, Downing JR, Baker SJ, Ellison DW and St. Jude Children's Research Hospital-Washington University Pediatric Cancer Genome Project: Whole-genome sequencing identifies genetic alterations in pediatric low-grade gliomas. Nat Genet *45(6)*: 602-612, 2013. PMID: 23583981. DOI: 10.1038/ng.2611

15 Jones DT, Hutter B, Jäger N, Korshunov A, Kool M, Warnatz HJ, Zichner T, Lambert SR, Ryzhova M, Quang DA, Fontebasso AM, Stütz AM, Hutter S, Zuckermann M, Sturm D, Gronych J, Lasitschka B, Schmidt S, Seker-Cin H, Witt H, Sultan M, Ralser M, Northcott PA, Hovestadt V, Bender S, Pfaff E, Stark S, Faury D, Schwartzentruber J, Majewski J, Weber UD, Zapatka M, Raeder B, Schlesner M, Worth CL, Bartholomae CC, von Kalle C, Imbusch CD, Radomski S, Lawerenz C, van Sluis P, Koster J, Volckmann R, Versteeg R, Lehrach H, Monoranu C, Winkler B, Unterberg A, Herold-Mende C, Milde T, Kulozik AE, Ebinger M, Schuhmann MU, Cho YJ, Pomeroy SL, von Deimling A, Witt O, Taylor MD, Wolf S, Karajannis MA, Eberhart CG, Scheurlen W, Hasselblatt M, Ligon KL, Kieran MW, Korbel JO, Yaspo ML, Brors B, Felsberg J, Reifenberger G, Collins VP, Jabado N, Eils R, Lichter P, Pfister SM and International Cancer Genome Consortium PedBrain Tumor Project: Recurrent somatic alterations of FGFR1 and NTRK2 in pilocytic astrocytoma. Nat Genet *45(8)*: 927-932, 2013. PMID: 23817572. DOI: 10.1038/ng.2682

16 Guerreiro Stucklin AS, Ryall S, Fukuoka K, Zapotocky M, Lassaletta A, Li C, Bridge T, Kim B, Arnoldo A, Kowalski PE, Zhong Y, Johnson M, Li C, Ramani AK, Siddaway R, Nobre LF, de Antonellis P, Dunham C, Cheng S, Boué DR, Finlay JL, Coven SL, de Prada I, Perez-Somarriba M, Faria CC, Grotzer MA, Rushing E, Sumerauer D, Zamecnik J, Krskova L, Garcia Ariza

M, Cruz O, Morales La Madrid A, Solano P, Terashima K, Nakano Y, Ichimura K, Nagane M, Sakamoto H, Gil-da-Costa MJ, Silva R, Johnston DL, Michaud J, Wilson B, van Landeghem FKH, Oviedo A, McNeely PD, Crooks B, Fried I, Zhukova N, Hansford JR, Nageswararao A, Garzia L, Shago M, Brudno M, Irwin MS, Bartels U, Ramaswamy V, Bouffet E, Taylor MD, Tabori U and Hawkins C: Alterations in ALK/ROS1/NTRK/MET drive a group of infantile hemispheric gliomas. Nat Commun *10(1)*: 4343, 2019. PMID: 31554817. DOI: 10.1038/s41467-019-12187-5

17 Clarke M, Mackay A, Ismer B, Pickles JC, Tatevossian RG, Newman S, Bale TA, Stoler I, Izquierdo E, Temelso S, Carvalho DM, Molinari V, Burford A, Howell L, Virasami A, Fairchild AR, Avery A, Chalker J, Kristiansen M, Haupfear K, Dalton JD, Orisme W, Wen J, Hubank M, Kurian KM, Rowe C, Maybury M, Crosier S, Knipstein J, Schüller U, Kordes U, Kram DE, Snuderl M, Bridges L, Martin AJ, Doey LJ, Al-Sarraj S, Chandler C, Zebian B, Cairns C, Natrajan R, Boult JKR, Robinson SP, Sill M, Dunkel IJ, Gilheeney SW, Rosenblum MK, Hughes D, Proszek PZ, Macdonald TJ, Preusser M, Haberler C, Slavc I, Packer R, Ng HK, Caspi S, Popović M, Faganel Kotnik B, Wood MD, Baird L, Davare MA, Solomon DA, Olsen TK, Brandal P, Farrell M, Cryan JB, Capra M, Karremann M, Schittenhelm J, Schuhmann MU, Ebinger M, Dinjens WNM, Kerl K, Hettmer S, Pietsch T, Andreiuolo F, Driever PH, Korshunov A, Hiddingh L, Worst BC, Sturm D, Zuckermann M, Witt O, Bloom T, Mitchell C, Miele E, Colafati GS, Diomedi-Camassei F, Bailey S, Moore AS, Hassall TEG, Lowis SP, Tsoli M, Cowley MJ, Ziegler DS, Karajannis MA, Aquilina K, Hargrave DR, Carceller F, Marshall LV, von Deimling A, Kramm CM, Pfister SM, Sahm F, Baker SJ, Mastronuzzi A, Carai A, Vinci M, Capper D, Popov S, Ellison DW, Jacques TS, Jones DTW and Jones C: Infant high-grade gliomas comprise multiple subgroups characterized by novel targetable gene fusions and favorable outcomes. Cancer Discov *10(7)*: 942-963, 2020. PMID: 32238360. DOI: 10.1158/2159-8290.CD-19-1030

18 Louis DN, Perry A, Wesseling P, Brat DJ, Cree IA, Figarella-Branger D, Hawkins C, Ng HK, Pfister SM, Reifenberger G, Soffietti R, von Deimling A and Ellison DW: The 2021 WHO classification of tumors of the central nervous system: a summary. Neuro Oncol *23(8)*: 1231-1251, 2021. PMID: 34185076. DOI: 10.1093/neuonc/noab106

19 Roskoski R Jr: Properties of FDA-approved small molecule protein kinase inhibitors: A 2022 update. Pharmacol Res *175*: 106037, 2022. PMID: 34921994. DOI: 10.1016/j.phrs.2021.106037

20 Freed D, Pan R and Aldana R: TNscope: Accurate detection of somatic mutations with haplotype-based variant candidate detection and machine learning filtering. biorxiv, 2019. DOI: 10.1101/250647

21 Roller E, Ivakhno S, Lee S, Royce T and Tanner S: Canvas: versatile and scalable detection of copy number variants. Bioinformatics *32(15)*: 2375-2377, 2016. PMID: 27153601. DOI: 10.1093/bioinformatics/btw163

22 Chen X, Schulz-Trieglaff O, Shaw R, Barnes B, Schlesinger F, Källberg M, Cox AJ, Kruglyak S and Saunders CT: Manta: rapid detection of structural variants and indels for germline and cancer sequencing applications. Bioinformatics *32(8)*: 1220-1222, 2016. PMID: 26647377. DOI: 10.1093/bioinformatics/btv710

23 Robinson JT, Thorvaldsdóttir H, Winckler W, Guttman M, Lander ES, Getz G and Mesirov JP: Integrative genomics viewer. Nat Biotechnol *29(1)*: 24-26, 2011. PMID: 21221095. DOI: 10.1038/nbt.1754

24 Nicorici D, Satalan M, Edgren H, Kangaspeska S, Murumagi A, Kallioniemi O, Virtanen S and Kilkku O: FusionCatcher - a tool for finding somatic fusion genes in paired-end RNA-sequencing data. biorxiv, 2020. DOI: 10.1101/011650

25 Langmead B and Salzberg SL: Fast gapped-read alignment with Bowtie 2. Nat Methods *9(4)*: 357-359, 2012. PMID: 22388286. DOI: 10.1038/nmeth.1923

26 Ferreyra Vega S, Olsson Bontell T, Corell A, Smits A, Jakola AS and Carén H: DNA methylation profiling for molecular classification of adult diffuse lower-grade gliomas. Clin Epigenetics *13(1)*: 102, 2021. PMID: 33941250. DOI: 10.1186/s13148-021-01085-7

27 Capper D, Jones DTW, Sill M, Hovestadt V, Schrimpf D, Sturm D, Koelsche C, Sahm F, Chavez L, Reuss DE, Kratz A, Wefers AK, Huang K, Pajtler KW, Schweizer L, Stichel D, Olar A, Engel NW, Lindenberg K, Harter PN, Braczynski AK, Plate KH, Dohmen H, Garvalov BK, Coras R, Hölsken A, Hewer E, Bewerunge-Hudler M, Schick M, Fischer R, Beschorner R, Schittenhelm J, Staszewski O, Wani K, Varlet P, Pages M, Temming P, Lohmann D, Selt F, Witt H, Milde T, Witt O, Aronica E, Giangaspero F, Rushing E, Scheurlen W, Geisenberger C, Rodriguez FJ, Becker A, Preusser M, Haberler C, Bjerkvig R, Cryan J, Farrell M, Deckert M, Hench J, Frank S, Serrano J, Kannan K, Tsirigos A, Brück W, Hofer S, Brehmer S, Seiz-Rosenhagen M, Hänggi D, Hans V, Rozsnoki S, Hansford JR, Kohlhof P, Kristensen BW, Lechner M, Lopes B, Mawrin C, Ketter R, Kulozik A, Khatib Z, Heppner F, Koch A, Jouvet A, Keohane C, Mühleisen H, Mueller W, Pohl U, Prinz M, Benner A, Zapatka M, Gottardo NG, Driever PH, Kramm CM, Müller HL, Rutkowski S, von Hoff K, Frühwald MC, Gnekow A, Fleischhack G, Tippelt S, Calaminus G, Monoranu CM, Perry A, Jones C, Jacques TS, Radlwimmer B, Gessi M, Pietsch T, Schramm J, Schackert G, Westphal M, Reifenberger G, Wesseling P, Weller M, Collins VP, Blümcke I, Bendszus M, Debus J, Huang A, Jabado N, Northcott PA, Paulus W, Gajjar A, Robinson GW, Taylor MD, Jaunmuktane Z, Ryzhova M, Platten M, Unterberg A, Wick W, Karajannis MA, Mittelbronn M, Acker T, Hartmann C, Aldape K, Schüller U, Buslei R, Lichter P, Kool M, Herold-Mende C, Ellison DW, Hasselblatt M, Snuderl M, Brandner S, Korshunov A, von Deimling A and Pfister SM: DNA methylation-based classification of central nervous system tumours. Nature *555(7697)*: 469-474, 2018. PMID: 29539639. DOI: 10.1038/nature26000

28 Crowe AR and Yue W: Semi-quantitative determination of protein expression using immunohistochemistry staining and analysis: an integrated protocol. Bio Protoc *9(24)*: e3465, 2019. PMID: 31867411. DOI: 10.21769/BioProtoc.3465

29 Drilon A, Jenkins C, Iyer S, Schoenfeld A, Keddy C and Davare MA: ROS1-dependent cancers - biology, diagnostics and therapeutics. Nat Rev Clin Oncol *18(1)*: 35-55, 2021. PMID: 32760015. DOI: 10.1038/s41571-020-0408-9

30 Uguen A and De Braekeleer M: ROS1 fusions in cancer: a review. Future Oncol *12(16)*: 1911-1928, 2016. PMID: 27256160. DOI: 10.2217/fon-2016-0050

31 Zhao S, Zhao ZJ, He HY, Wu JC, Ding XQ, Yang L, Jia N, Li ZJ and Zheng HC: The roles of ING5 in gliomas: a good marker for tumorigenesis and a potential target for gene therapy. Oncotarget *8(34)*: 56558-56568, 2017. PMID: 28915612. DOI: 10.18632/oncotarget.17802

32 Della-Valle V, Roos-Weil D, Scourzic L, Mouly E, Aid Z, Darwiche W, Lecluse Y, Damm F, Mémet S, Mercher T, Aoufouchi S, Nguyen-Khac F, Bernard OA and Ghamlouch H: Nfkbie-deficiency leads to increased susceptibility to develop B-

cell lymphoproliferative disorders in aged mice. Blood Cancer J *10(3)*: 38, 2020. PMID: 32170099. DOI: 10.1038/s41408-020-0305-6

33 Snow CJ and Paschal BM: Roles of the nucleoporin Tpr in cancer and aging. Adv Exp Med Biol *773*: 309-322, 2014. PMID: 24563354. DOI: 10.1007/978-1-4899-8032-8_14

34 Choi YL, Lira ME, Hong M, Kim RN, Choi SJ, Song JY, Pandy K, Mann DL, Stahl JA, Peckham HE, Zheng Z, Han J, Mao M and Kim J: A novel fusion of TPR and ALK in lung adenocarcinoma. J Thorac Oncol *9(4)*: 563-566, 2014. PMID: 24736082. DOI: 10.1097/JTO.0000000000000093

35 Kim SY, Kim JE, Park S and Kim HK: Molecular identification of a TPR-FGFR1 fusion transcript in an adult with myeloproliferative neoplasm, T-lymphoblastic lymphoma, and a t(1;8)(q25;p11.2). Cancer Genet *207(6)*: 258-262, 2014. PMID: 25037443. DOI: 10.1016/j.cancergen.2014.05.011

36 Rekhi B, Shetty O, Bapat P, Gurav M and Qureshi S: A case of Inv(1)(q23q31) *TPR-NTRK1* fusion-positive spindle cell neoplasm in an infant-uncovered by next-generation sequencing: diagnostic challenge, review, and therapeutic implications. Int J Surg Pathol *29(1)*: 102-108, 2021. PMID: 32489127. DOI: 10.1177/1066896920927467

37 Al-Ibraheemi A, Folpe AL, Perez-Atayde AR, Perry K, Hofvander J, Arbajian E, Magnusson L, Nilsson J and Mertens F: Aberrant receptor tyrosine kinase signaling in lipofibromatosis: a clinicopathological and molecular genetic study of 20 cases. Mod Pathol *32(3)*: 423-434, 2019. PMID: 30310176. DOI: 10.1038/s41379-018-0150-3

38 Cooper CS, Park M, Blair DG, Tainsky MA, Huebner K, Croce CM and Vande Woude GF: Molecular cloning of a new transforming gene from a chemically transformed human cell line. Nature *311(5981)*: 29-33, 1984. PMID: 6590967. DOI: 10.1038/311029a0

39 Soman NR, Correa P, Ruiz BA and Wogan GN: The TPR-MET oncogenic rearrangement is present and expressed in human gastric carcinoma and precursor lesions. Proc Natl Acad Sci U S A *88(11)*: 4892-4896, 1991. PMID: 2052572. DOI: 10.1073/pnas.88.11.4892

40 Greco A, Pierotti MA, Bongarzone I, Pagliardini S, Lanzi C and Della Porta G: TRK-T1 is a novel oncogene formed by the fusion of TPR and TRK genes in human papillary thyroid carcinomas. Oncogene *7(2)*: 237-242, 1992. PMID: 1532241.

41 Takeuchi K, Soda M, Togashi Y, Suzuki R, Sakata S, Hatano S, Asaka R, Hamanaka W, Ninomiya H, Uehara H, Lim Choi Y, Satoh Y, Okumura S, Nakagawa K, Mano H and Ishikawa Y: RET, ROS1 and ALK fusions in lung cancer. Nat Med *18(3)*: 378-381, 2012. PMID: 22327623. DOI: 10.1038/nm.2658

42 Zhao S, Zhu S, Lei X, Xu D, Shi T, Chen Q, Ren F, Chen G, Huang D and Xu S: Use of crizotinib as neoadjuvant therapy for non-small cell lung cancers patient with ROS1 rearrangement: A case report. Thorac Cancer *12(20)*: 2815-2818, 2021. PMID: 34405544. DOI: 10.1111/1759-7714.14112

43 Qiu JJ, Chu H, Lu X, Jiang X and Dong S: The reduced and altered activities of PAX5 are linked to the protein-protein interaction motif (coiled-coil domain) of the PAX5-PML fusion protein in t(9;15)-associated acute lymphocytic leukemia. Oncogene *30(8)*: 967-977, 2011. PMID: 20972455. DOI: 10.1038/onc.2010.473

44 Kang J, Park JW, Won JK, Bae JM, Koh J, Yim J, Yun H, Kim SK, Choi JY, Kang HJ, Kim WS, Shin JH and Park SH: Clinicopathological findings of pediatric NTRK fusion mesenchymal tumors. Diagn Pathol *15(1)*: 114, 2020. PMID: 32957984. DOI: 10.1186/s13000-020-01031-w

45 Atiq MA, Davis JL, Hornick JL, Dickson BC, Fletcher CDM, Fletcher JA, Folpe AL and Mariño-Enríquez A: Mesenchymal tumors of the gastrointestinal tract with NTRK rearrangements: a clinicopathological, immunophenotypic, and molecular study of eight cases, emphasizing their distinction from gastrointestinal stromal tumor (GIST). Mod Pathol *34(1)*: 95-103, 2021. PMID: 32669612. DOI: 10.1038/s41379-020-0623-z

46 Pekova B, Sykorova V, Dvorakova S, Vaclavikova E, Moravcova J, Katra R, Astl J, Vlcek P, Kodetova D, Vcelak J and Bendlova B: *RET*, *NTRK*, *ALK*, *BRAF*, and *MET* fusions in a large cohort of pediatric papillary thyroid carcinomas. Thyroid *30(12)*: 1771-1780, 2020. PMID: 32495721. DOI: 10.1089/thy.2019.0802

47 Kim M, Jeong JY, Park NJ and Park JY: Clinical utility of next-generation sequencing in real-world cases: a single-institution study of nine cases. In Vivo *36(3)*: 1397-1407, 2022. PMID: 35478134. DOI: 10.21873/invivo.12844

48 Uhlén M, Fagerberg L, Hallström BM, Lindskog C, Oksvold P, Mardinoglu A, Sivertsson Å, Kampf C, Sjöstedt E, Asplund A, Olsson I, Edlund K, Lundberg E, Navani S, Szigyarto CA, Odeberg J, Djureinovic D, Takanen JO, Hober S, Alm T, Edqvist PH, Berling H, Tegel H, Mulder J, Rockberg J, Nilsson P, Schwenk JM, Hamsten M, von Feilitzen K, Forsberg M, Persson L, Johansson F, Zwahlen M, von Heijne G, Nielsen J and Pontén F: Proteomics. Tissue-based map of the human proteome. Science *347(6220)*: 1260419, 2015. PMID: 25613900. DOI: 10.1126/science.1260419

49 Charest A, Wilker EW, McLaughlin ME, Lane K, Gowda R, Coven S, McMahon K, Kovach S, Feng Y, Yaffe MB, Jacks T and Housman D: ROS fusion tyrosine kinase activates a SH2 domain-containing phosphatase-2/phosphatidylinositol 3-kinase/mammalian target of rapamycin signaling axis to form glioblastoma in mice. Cancer Res *66(15)*: 7473-7481, 2006. PMID: 16885344. DOI: 10.1158/0008-5472.CAN-06-1193

50 Mendoza MC, Er EE and Blenis J: The Ras-ERK and PI3K-mTOR pathways: cross-talk and compensation. Trends Biochem Sci *36(6)*: 320-328, 2011. PMID: 21531565. DOI: 10.1016/j.tibs.2011.03.006

51 Yi YW, You KS, Park JS, Lee SG and Seong YS: Ribosomal protein S6: a potential therapeutic target against cancer? Int J Mol Sci *23(1)*: 48, 2021. PMID: 35008473. DOI: 10.3390/ijms23010048

52 Capizzi E, Dall'Olio FG, Gruppioni E, Sperandi F, Altimari A, Giunchi F, Fiorentino M and Ardizzoni A: Clinical significance of ROS1 5' deletions in non-small cell lung cancer. Lung Cancer *135*: 88-91, 2019. PMID: 31447007. DOI: 10.1016/j.lungcan.2019.07.017

53 Mahipal A, Kommalapati A, Tella SH, Lim A and Kim R: Novel targeted treatment options for advanced cholangiocarcinoma. Expert Opin Investig Drugs *27(9)*: 709-720, 2018. PMID: 30124336. DOI: 10.1080/13543784.2018.1512581

54 Gendarme S, Bylicki O, Chouaid C and Guisier F: *ROS-1* fusions in non-small-cell lung cancer: evidence to date. Curr Oncol *29(2)*: 641-658, 2022. PMID: 35200557. DOI: 10.3390/curroncol29020057

55 Johnson A, Severson E, Gay L, Vergilio JA, Elvin J, Suh J, Daniel S, Covert M, Frampton GM, Hsu S, Lesser GJ, Stogner-Underwood K, Mott RT, Rush SZ, Stanke JJ, Dahiya S, Sun J, Reddy P, Chalmers ZR, Erlich R, Chudnovsky Y, Fabrizio D, Schrock AB, Ali S, Miller V, Stephens PJ, Ross J, Crawford JR and Ramkissoon SH: Comprehensive genomic profiling of 282

pediatric low- and high-grade gliomas reveals genomic drivers, tumor mutational burden, and hypermutation signatures. Oncologist *22(12)*: 1478-1490, 2017. PMID: 28912153. DOI: 10.1634/theoncologist.2017-0242

56 Nakano Y, Tomiyama A, Kohno T, Yoshida A, Yamasaki K, Ozawa T, Fukuoka K, Fukushima H, Inoue T, Hara J, Sakamoto H and Ichimura K: Identification of a novel KLC1-ROS1 fusion in a case of pediatric low-grade localized glioma. Brain Tumor Pathol *36(1)*: 14-19, 2019. PMID: 30350109. DOI: 10.1007/s10014-018-0330-3

57 El-Ayadi M, Ansari M, Sturm D, Gielen GH, Warmuth-Metz M, Kramm CM and von Bueren AO: High-grade glioma in very young children: a rare and particular patient population. Oncotarget *8(38)*: 64564-64578, 2017. PMID: 28969094. DOI: 10.18632/oncotarget.18478

58 Capper D, Jones DTW, Sill M, Hovestadt V, Schrimpf D, Sturm D, Koelsche C, Sahm F, Chavez L, Reuss DE, Kratz A, Wefers AK, Huang K, Pajtler KW, Schweizer L, Stichel D, Olar A, Engel NW, Lindenberg K, Harter PN, Braczynski AK, Plate KH, Dohmen H, Garvalov BK, Coras R, Hölsken A, Hewer E, Bewerunge-Hudler M, Schick M, Fischer R, Beschorner R, Schittenhelm J, Staszewski O, Wani K, Varlet P, Pages M, Temming P, Lohmann D, Selt F, Witt H, Milde T, Witt O, Aronica E, Giangaspero F, Rushing E, Scheurlen W, Geisenberger C, Rodriguez FJ, Becker A, Preusser M, Haberler C, Bjerkvig R, Cryan J, Farrell M, Deckert M, Hench J, Frank S, Serrano J, Kannan K, Tsirigos A, Brück W, Hofer S, Brehmer S, Seiz-Rosenhagen M, Hänggi D, Hans V, Rozsnoki S, Hansford JR, Kohlhof P, Kristensen BW, Lechner M, Lopes B, Mawrin C, Ketter R, Kulozik A, Khatib Z, Heppner F, Koch A, Jouvet A, Keohane C, Mühleisen H, Mueller W, Pohl U, Prinz M, Benner A, Zapatka M, Gottardo NG, Driever PH, Kramm CM, Müller HL, Rutkowski S, von Hoff K, Frühwald MC, Gnekow A, Fleischhack G, Tippelt S, Calaminus G, Monoranu CM, Perry A, Jones C, Jacques TS, Radlwimmer B, Gessi M, Pietsch T, Schramm J, Schackert G, Westphal M, Reifenberger G, Wesseling P, Weller M, Collins VP, Blümcke I, Bendszus M, Debus J, Huang A, Jabado N, Northcott PA, Paulus W, Gajjar A, Robinson GW, Taylor MD, Jaunmuktane Z, Ryzhova M, Platten M, Unterberg A, Wick W, Karajannis MA, Mittelbronn M, Acker T, Hartmann C, Aldape K, Schüller U, Buslei R, Lichter P, Kool M, Herold-Mende C, Ellison DW, Hasselblatt M, Snuderl M, Brandner S, Korshunov A, von Deimling A and Pfister SM: DNA methylation-based classification of central nervous system tumours. Nature *555(7697)*: 469-474, 2018. PMID: 29539639. DOI: 10.1038/nature26000

59 WHO Classification of Tumours Editorial Board (ed.): WHO Classification of Tumours, Central Nervous System Tumours, 5 edn. IARC Publications, pp. 81, 2021.

60 Rallis KS, George AM, Wozniak AM, Bigogno CM, Chow B, Hanrahan JG and Sideris M: Molecular genetics and targeted therapies for paediatric high-grade glioma. Cancer Genomics Proteomics *19(4)*: 390-414, 2022. PMID: 35732328. DOI: 10.21873/cgp.20328

61 Deland L, Keane S, Olsson Bontell T, Sjögren H, Fagman H, Øra I, De La Cuesta E, Tisell M, Nilsson JA, Ejeskär K, Sabel M and Abel F: Discovery of a rare *GKAP1-NTRK2* fusion in a pediatric low-grade glioma, leading to targeted treatment with TRK-inhibitor larotrectinib. Cancer Biol Ther *22(3)*: 184-195, 2021. PMID: 33820494. DOI: 10.1080/15384047.2021.1899573

62 Pollack IF, Agnihotri S and Broniscer A: Childhood brain tumors: current management, biological insights, and future directions. J Neurosurg Pediatr *23(3)*: 261-273, 2019. PMID: 30835699. DOI: 10.3171/2018.10.PEDS18377

63 Packer RJ, Pfister S, Bouffet E, Avery R, Bandopadhayay P, Bornhorst M, Bowers DC, Ellison D, Fangusaro J, Foreman N, Fouladi M, Gajjar A, Haas-Kogan D, Hawkins C, Ho CY, Hwang E, Jabado N, Kilburn LB, Lassaletta A, Ligon KL, Massimino M, Meeteren SV, Mueller S, Nicolaides T, Perilongo G, Tabori U, Vezina G, Warren K, Witt O, Zhu Y, Jones DT and Kieran M: Pediatric low-grade gliomas: implications of the biologic era. Neuro Oncol *19(6)*: 750-761, 2017. PMID: 27683733. DOI: 10.1093/neuonc/now209

64 Landi L and Cappuzzo F: How selecting best upfront therapy for metastatic disease?-Focus on ROS1-rearranged disease. Transl Lung Cancer Res *9(6)*: 2686-2695, 2020. PMID: 33489827. DOI: 10.21037/tlcr-20-1109

65 Drilon A, Ou SI, Cho BC, Kim DW, Lee J, Lin JJ, Zhu VW, Ahn MJ, Camidge DR, Nguyen J, Zhai D, Deng W, Huang Z, Rogers E, Liu J, Whitten J, Lim JK, Stopatschinskaja S, Hyman DM, Doebele RC, Cui JJ and Shaw AT: Repotrectinib (TPX-0005) is a next-generation ROS1/TRK/ALK inhibitor that potently inhibits ROS1/TRK/ALK solvent- front mutations. Cancer Discov *8(10)*: 1227-1236, 2018. PMID: 30093503. DOI: 10.1158/2159-8290.CD-18-0484

66 Indini A, Rijavec E, Ghidini M, Bareggi C, Gambini D, Galassi B, Antonelli P, Bettio G, Di Nubila C and Grossi F: Pharmacotherapeutic advances with anaplastic lymphoma kinase inhibitors for the treatment of non-small cell lung cancer. Expert Opin Pharmacother *21(8)*: 931-940, 2020. PMID: 32162559. DOI: 10.1080/14656566.2020.1738387

67 Li T, Ma W and Tian EC: Ensartinib (X-396): what does it add for patients with ALK-rearranged NSCLC. Chin Clin Oncol *8(S1)*: S4, 2019. PMID: 30525756. DOI: 10.21037/cco.2018.10.12

68 Lee J, Park S, Jung HA, Sun JM, Lee SH, Ahn JS, Park K and Ahn MJ: Evaluating entrectinib as a treatment option for non-small cell lung cancer. Expert Opin Pharmacother *21(16)*: 1935-1942, 2020. PMID: 32736487. DOI: 10.1080/14656566.2020.1798932

Received June 27, 2022
Revised August 8, 2022
Accepted August 22, 2022